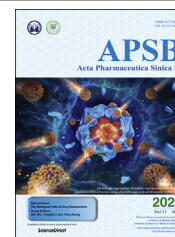




Chinese Pharmaceutical Association
Institute of Materia Medica, Chinese Academy of Medical Sciences

Acta Pharmaceutica Sinica B

www.elsevier.com/locate/apsb
www.sciencedirect.com



ORIGINAL ARTICLE

In vivo dissolution of poorly water-soluble drugs: Proof of concept based on fluorescence bioimaging



Yinqian Yang^a, Yongjiu Lv^a, Chengying Shen^a, Tingting Shi^a,
Haisheng He^a, Jianping Qi^a, Xiaochun Dong^a, Weili Zhao^a, Yi Lu^a,
Wei Wu^{a,b,*}

^aKey Laboratory of Smart Drug Delivery of MOE, School of Pharmacy, Fudan University, Shanghai 201203, China

^bCenter for Medical Research and Innovation, Shanghai Pudong Hospital, Fudan University Pudong Medical Center, Shanghai 201399, China

Received 18 April 2020; received in revised form 16 June 2020; accepted 9 July 2020

KEY WORDS

In vivo dissolution;
Fenofibrate;
Fluorescence;
Aggregation-caused
quenching;
Bioimaging;
IVIVC

Abstract *In vitro*–*in vivo* correlation (IVIVC) of solid dosage forms should be established basically between *in vitro* and *in vivo* dissolution of active pharmaceutical ingredients. Nevertheless, *in vivo* dissolution profiles have never been accurately portrayed. The current practice of IVIVC has to resort to *in vivo* absorption fractions (F_a). In this proof-of-concept study, *in vivo* dissolution of a model poorly water-soluble drug fenofibrate (FNB) was investigated by fluorescence bioimaging. FNB crystals were first labeled by near-infrared fluorophores with aggregation-caused quenching properties. The dyes illuminated FNB crystals but quenched immediately and absolutely once been released into aqueous media, enabling accurate monitoring of residual drug crystals. The linearity established between fluorescence and crystal concentration justified reliable quantification of FNB crystals. *In vitro* dissolution was first measured following pharmacopoeia monograph protocols with well-documented IVIVC. The synchronicity between fluorescence and *in vitro* dissolution of FNB supported using fluorescence as a measure for determination of dissolution. *In vitro* dissolution correlated well with *in vivo* dissolution, acquired by either live or *ex vivo* imaging. The newly established IVIVC was further validated by correlating both *in vitro* and *in vivo* dissolution with F_a obtained from pharmacokinetic data.

*Corresponding author.

E-mail address: wuwei@shmu.edu.cn (Wei Wu).

Peer review under responsibility of Chinese Pharmaceutical Association and Institute of Materia Medica, Chinese Academy of Medical Sciences.

<https://doi.org/10.1016/j.apsb.2020.08.002>

2211-3835 © 2021 Chinese Pharmaceutical Association and Institute of Materia Medica, Chinese Academy of Medical Sciences. Production and hosting by Elsevier B.V. This is an open access article under the CC BY-NC-ND license (<http://creativecommons.org/licenses/by-nc-nd/4.0/>).

1. Introduction

Active pharmaceutical ingredients (APIs) intended for oral administration are preferably formulated as solid dosage forms, which are principally comprised of drug particles—in either crystalline or amorphous form—and excipients, such as tablets and capsules, owing to stability considerations and ease of manufacturing, transportation, storage and administration. Solid dosage forms, except those meant for sustained or controlled release, are generally designed to disintegrate rapidly in the gastrointestinal tract (GIT) to liberate drug particles, which further dissolve to present the drugs in a solubilized state¹. Drug molecules are thereafter absorbed across the enteric epithelia *via* different mechanisms—passive diffusion, facilitated diffusion or energy-consuming active transport². Drug particles *per se*—generally in the size range of a few to a few tens of microns—are unable to be absorbed *via* the enteric epithelia. Despite recent reports of oral absorption of minute amount of drug particles with a size of several hundred nanometers^{3–6}, a majority of drugs are absorbed in a molecularly dissolved state. The dissolution of drug particles following disintegration of solid dosage forms is one of the rate-limiting steps that determine the overall absorption rate and content^{7–9}.

The exploration of *in vivo* dissolution digs information crucial for the understanding of drug absorption. It can be employed to guide not only the establishment of *in vitro* dissolution protocols but also the development of formulations. Unfortunately, the virtual *in vivo* dissolution profile of any drugs has never been accurately determined due to a lack of functional tools to monitor changes in total amount of dissolved drugs or residual drug particles continuously in the GIT. A great deal of time and money has been wasted on tedious formulation optimization without the guidance of *in vivo* dissolution¹⁰. The current *in vitro* dissolution protocols, which should stem from *in vivo* dissolution, have been established merely on the basis of *in vitro* observations and experience. Monograph *in vitro* dissolution test so far serves well as a measure to inspect formulation conformity but perform awkwardly to predict *in vivo* performance. In order to elevate the eligibility of *in vitro* dissolution test, bio-relevant media have been widely utilized to mimic *in vivo* conditions^{11–14}. However, *in vitro*–*in vivo* correlation (IVIVC) should be established to justify *in vitro* dissolution test^{15–17}. Paradoxically, the establishment of IVIVC calls for *in vivo* dissolution data^{18–20}. Since *in vivo* dissolution cannot be measured accurately at the moment, previous establishment of IVIVC has to resort to *in vivo* absorption fractions (F_a)^{20–22}, presuming that certain correlation between F_a and *in vivo* dissolution can be built. Fig. 1 is a schematic demonstration of the correlation among *in vitro* dissolution, *in vivo* dissolution and F_a . The calculation of F_a is based on deconvolution of plasma pharmacokinetic data by the Wagner–Nelson or Riegelman–Loo method^{17,23–25}. The deconvolution approach assumes linear absorption into and elimination from the circulation,

which however is often biased, especially for poorly permeable drugs such as Class III and Class IV compounds under Biopharmaceutics Classification System (BCS), compromising the establishment of IVIVC²⁶. So far, the overall acceptance rate of all IVIVC studies is very low. For instance, only 40% for all submissions to U.S. Food and Drug Administration (FDA)^{17,27–29}. The European Innovative Medicines Initiative and FDA launched major research projects—the OrBiTo (oral biopharmaceutical tools) and the 21st Century BA/BE, respectively—to establish *in vitro/in silico* tools to predict *in vivo* drug behaviors so as to elevate the success rate of IVIVC^{10,13,30,31}. The complex and variable gastrointestinal conditions compromise the accuracy of these tools^{32–34}.

Basically, IVIVC should be established between *in vitro* and *in vivo* dissolution. It is because *in vivo* dissolution data are not available that F_a has been employed as a makeshift substitute to establish IVIVC. Difficult as it is, measurement of *in vivo* dissolution has been tried before. An intraluminal sampling technique utilizing a long multichannel tube (Loc-I-Gut) was developed to detect drug levels directly in the GIT^{35–37}. Although the technique enables simultaneous aspiration of both gastric and intestinal fluids, its drawbacks are equally apparent. Unlike in *in vitro* dissolution media, drugs are non-uniformly distributed in the GIT. It is impractical to get a panoramic view of drug dissolution by sampling at a fixed position. Dissolution of undissolved drug particles continues during separation of the aspirated fluids as well, while the processing—by for example centrifugation and ultrafiltration—may accelerate dissolution³⁸. In addition, the invasive sampling catheter may cause duodenogastric reflux³⁹. All of the disadvantages compromise the accuracy of the sampling strategy. As a result, only changes in drug concentrations are recorded and it is impossible to draw an *in vivo* dissolution profile based on the intraluminal sampling technique. Instead of measuring dissolved drugs, undissolved drug particles can be measured following intraluminal sampling in human GIT, too⁴⁰. However, the same drawbacks as measuring dissolved drugs exist.

In this proof-of-concept study, a novel strategy is implemented to measure *in vivo* drug dissolution by real-time monitoring of residual particles in the GIT based on fluorescence live imaging in rats. In the previous studies, we made the first step to identify crystalline or amorphous drug nanoparticles *in vivo* after labeling with near-infrared fluorophores using the hybridized drug crystallization technique^{5,6}. The dyes bear a BODIPY or an aza-BODIPY parent structure and emit fluorescence when molecularly dispersed (“on”)^{41,42}. Unlike conventional fluorophores^{43–47}, the fluorescence of this kind of dyes quenches immediately and completely (“off”) upon nanocrystal dissolution and dye release into aqueous media, as dye molecules aggregate *via* π – π stacking, a phenomenon commonly known as aggregation-caused quenching (ACQ) in fluorescence bioimaging^{48–50}. Therefore, the fluorescence signals can be used to represent undissolved nanocrystals. By exploiting the “on-to-off” signal switching

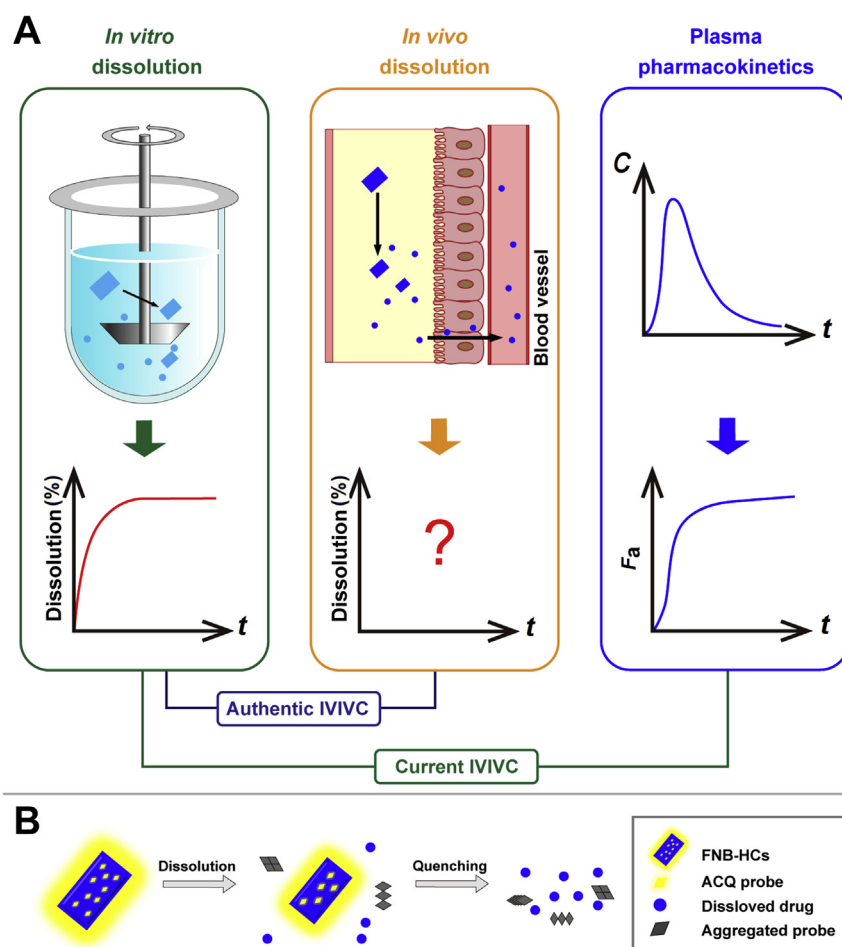


Figure 1 Schematic demonstration of correlation among *in vitro* dissolution, *in vivo* dissolution and absorption fraction of drug crystals (A), and the rationale of the ACQ-based fluorescent bioimaging of fenofibrate crystals (B). Current IVIVC is established between *in vitro* dissolution and F_a as a makeshift. Nevertheless, authentic IVIVC should be established between *in vitro* and *in vivo* dissolution.

feature of ACQ dyes, the *in vivo* fate of a series of nanocarriers has been explored *via* different administration routes^{51–53}.

Herein, fenofibrate (FNB), a Class II compound under BCS, was utilized as a model drug to testify the concept of *in vivo* dissolution, because of well-established IVIVC^{22,54–56}. An ACQ dye with an aza-BODIPY parent structure, P2, was embedded into the lattices of FNB crystals to prepare fluorescently hybridized FNB crystals (FNB–HCs). *In vivo* dissolution was investigated by real-time live imaging and correlated to *in vitro* dissolution. To validate the *in vivo* dissolution model, *in vivo* F_a calculated from pharmacokinetic data was employed to perform correlation with both *in vitro* and *in vivo* dissolution.

2. Materials and methods

2.1. Materials

FNB was purchased from Xuzhou Enhua pharmaceutical Co., Ltd. (Xuzhou, China). HPMC-E5 was provided by Shanghai Colorcon Coating Technology Co., Ltd. (Shanghai, China). ACQ dye P2 ($\lambda_{\text{abs}}/\lambda_{\text{em}} = 708 \text{ nm}/732 \text{ nm}$) was synthesized in our laboratory according to previous procedures^{57,58}. Powders for reconstitution of biorelevant gastrointestinal fluids were obtained from

Biorelevant. Com Ltd. (Croydon, UK). Isoflurane was obtained from Shandong Keyuan Pharmaceutical Co., Ltd. (Jinan, China). Deionized water was prepared by a Milli-Q® (Millipore, Molsheim, France) water purification system, filtered through 0.2 μm membrane and used in all experiments.

Male Sprague–Dawley (SD) rats, weighing $200 \pm 20 \text{ g}$, were obtained from Shanghai Laboratory Animal Center (Shanghai, China). All experimental procedures involving use of animals were approved by the Institutional Animal Care and Use Committee at School of Pharmacy, Fudan University, China.

2.2. Preparation of FNB-HCs

FNB-HCs were prepared using an anti-solvent crystallization method with modifications⁵⁹. The effects of stirring speed, solvent volume and drug concentration on particle size and span of size distribution were screened (Supporting Information Fig. S1). Briefly, both P2 (80 μg) and FNB (60 mg) were first dissolved in 1 mL ethanol. The ethanol solution was then poured rapidly into 50 mL HPMC-E5 aqueous solution (0.04%, w/v) under stirring and stirred continuously at a speed of 700 rpm for 5 min (IKA® RW20 Digital, Staufen, Germany). The suspensions obtained were filtered through a 220 nm polycarbonate membrane

(Sigma–Aldrich, St. Louis, MO, USA), while the precipitates were rinsed with 50 mL water to remove residual HPMC-E5. FNB-HCs were collected after drying the precipitates at room temperature under vacuum.

2.3. Characterization of FNB-HCs

For measurement of particle size, span and fluorescence intensity, FNB-HCs were suspended in water under ultrasonication (Ningbo Xinzhi biotechnology Co., Ltd., China) to an FNB concentration of 12 mg/mL. The particle size and span were determined by a Malvern Mastersizer 3000 laser particle analyzer (Malvern instrument, Malvern, UK) at room temperature. The operating conditions were set as follows: refractive index 1.52; absorption rate 0.1; density 1 g/cm³; shading limit 0.5%–5%. The FNB-HC suspensions (200 µL) were instilled into 96-well plates for measurement of fluorescence intensity using IVIS Spectrum Live Imaging System (PerkinElmer, Waltham, MA, USA) by a region of interest (ROI) quantification method^{49,50}.

For measurement of the encapsulation efficiency (EE, %) and drug loading (DL, %) of P2, 10 mg FNB-HCs were dissolved in 3 mL ethanol, and the fluorescence intensity of P2 was measured by a Cary Eclipse fluorescence spectrophotometer (Agilent, Santa Clara, CA, USA). The loading amount of P2 was measured by a pre-established calibration curve based on the fluorescence intensity of P2 measured in ethanol. The EE (%) and DL (%) were calculated by the following Eqs. (1) and (2):

$$EE (\%) = \text{Amount of P2 loaded} / \text{Amount of P2 added} \times 100 \quad (1)$$

$$DL (\%) = \text{Amount of P2 loaded} / \text{Amount of FNB - HCs} \times 100 \quad (2)$$

The morphology of FNB-HCs, as well as FNB raw materials, was observed by an SU8000 scanning electron microscopy (SEM, Hitachi, Tokyo, Japan). The solid samples were sputter coated with a conductive layer of gold palladium and observed at an accelerating excitation voltage of 10 kV. The differential scanning calorimetry (DSC) thermograms were collected using a 204A/G thermal analyser (Netzsch, Bühl, Germany) at a heating speed of 5 °C/min from 50 to 165 °C under a nitrogen gas flow of 30 mL/min. The powder X-ray diffractometry (PXRD) patterns of the same samples were recorded by a D/MAX-2500/PC X-ray diffractometer (Rigaku, Tokyo, Japan) with a Cu source of radiation over the 2θ range from 7° to 45°, with a step angle of 0.02° and counting frequency of 2°/min.

2.4. Fluorescence stability of FNB-HCs

The fluorescence stability of FNB-HCs in water, buffers of different pHs and simulated physiological media was investigated to assess dye leakage or premature water infiltration into the crystals lattices, all of which may result in interference to live imaging^{5,6,42}. During the experiment, FNB-HCs were suspended in 10 mL of the medium to a concentration of 2.4 mg/mL and incubated at 37 °C. Samples were withdrawn at 0, 0.5, 1.0, 1.5, 2.0, 3.0, 4.0, 6.0, 8.0 and 12.0 h, respectively, and measured for fluorescence intensity by a fluorescence spectrophotometer.

2.5. Fluorescence quenching sensitivity to water

In the previous study⁴⁸, the ACQ effect of the dye P2 was investigated by observing the fluorescence intensity as a function of water content in a binary acetonitrile/water system. In this study, the same experiment was performed on FNB-HCs, but using an ethanol/water system instead to make sure that FNB crystals could dissolve quickly enough. A series of aqueous ethanol with varied water contents in the range of 1%–99% (*v/v*) were prepared. Then, 10 µL FNB-HC suspension (12 mg/mL) were dissolved in 40 mL aqueous ethanol. The fluorescence spectra were scanned by a fluorescence spectrophotometer at an excitation wavelength of 690 nm and emission wavelength range of 710–800 nm. The spectral slits were set to 10 nm.

2.6. Quantification of FNB-HCs in dissolution media

A calibration curve was established between fluorescence intensity and concentration of FNB-HCs. The fluorescence intensity of FNB-HC suspensions with a series of concentrations were measured using a fluorescence spectrophotometer. In parallel, 1 mL of the suspensions was dissolved in methanol and diluted to 50 mL to determine the concentration of FNB by Agilent 1260 series HPLC system (Agilent). The correlation between fluorescence intensity and concentration of FNB-HCs was established. The precision and accuracy of the assay were evaluated at high, medium and low levels of FNB-HCs, respectively (Supporting Information Fig. S2, Tables S1 and S2).

2.7. *In vitro* dissolution

In vitro dissolution of FNB-HCs was studied using a ZRS-8G dissolution tester (Tianjin, China) following ChP II (the paddle method) monograph procedures for evaluation of FNB formulations, which have been validated with good IVIVC (*in vitro* dissolution vs. F_a)⁶⁰. Sodium dodecyl sulfate aqueous solution (0.05 mol/L, 1000 mL) was utilized as the dissolution media to set a sink condition. The rotation speed was set to 50 rpm, while samples equivalent to 12 mg of FNB (1 mL suspension) were directly instilled into the beaker. At predetermined intervals, 2 mL samples were withdrawn and equal volume of blank media was compensated immediately. The fluorescence intensity of the samples was measured immediately using a fluorescence spectrophotometer. The percentage of residual fluorescence intensity was obtained by setting the initial fluorescence intensity as 100%. The fluorescence intensity of each sample was also substituted into the calibration curve to calculate the residual percentage of FNB-HCs (corrected). In the meantime, the dissolution samples were filtered through 0.22 µm PES membrane (Fine Scientific Ltd., Toronto, Canada) and assayed for FNB by HPLC. The accumulated percentage of dissolved FNB was subtracted from 100% to get the percentage of residual FNB-HCs. For ease of comparison, *in vitro* dissolution profiles were displayed as the percentages of residual FNB-HCs vs. time plots.

2.8. *In vivo* dissolution

Before the experiment, depilatory cream was applied to remove the hair on the abdominal side to reduce hair-derived auto-fluorescence. Since FNB exhibits high inter-individual variation under fasted state, the formulation is administered after a meal due to the pronounced food effects⁶¹. The animals were placed in individual

cages and allowed free access to food and water before experiment. The animals were randomly divided into two groups, and treated with FNB-HCs and quenched P2 dispersion as a control, respectively. Suspension equivalent to 12 mg FNB (1 mL) was administered to the rats by gavage. Epi-Illumination mode was used for IVIS scanning with excitation/emission wavelengths set to 710 nm/760 nm to capture P2 signals post administration. An on-line gas anesthetizing system using isoflurane was used to anaesthetize the rats during the imaging process. Fluorescence intensity measured instantly after administration was set as 100%, while the percentages of residual fluorescence intensity vs. time was plotted to depict the *in vivo* dissolution profiles.

Owing to the poor penetration of fluorescence, the whole GIT was dissected and observed *ex vivo* using the IVIS system. In brief, the animals were raised and administered with the test samples following the same procedures as for live imaging. At each time point, three animals were sacrificed by cervical dislocation and the gastrointestinal tissues were collected and imaged. The percentage of residual fluorescence intensity in *ex vivo* tissues was recorded. The dissolution profiles obtained *ex vivo* were compared with the *in vivo* profiles.

2.9. Validation by F_a -based IVIVC

To study the pharmacokinetics of FNB-HCs, 1 mL suspension equivalent to 12 mg FNB was administered to the rats by gavage. Blood samples (500 μ L) were withdrawn into heparinized test tubes from the eye socket vein pre-dosing (0 h) and at time intervals of 0.083, 0.167, 0.333, 0.5, 0.75, 1, 1.5, 2, 3, 4, 6, 8, 10, 12, 16 and 24 h post-dosing. Plasma was collected after centrifugation (Anke TGL-16G, Shanghai, China) of the blood samples at 3000 rpm for 5 min and stored at -20°C for subsequent analysis. Since FNB is rapidly metabolized into fenofibric acid in blood, the pharmacokinetics of FNB was evaluated based on monitoring of fenofibric acid⁶². Fenofibric acid in rat plasma was extracted by liquid–liquid extraction following procedures established in a previous study⁶³. The method development and validation details are shown in the Supporting Information. Pharmacokinetic parameters were calculated by DAS 2.0 (Shanghai Bioguided Medicinal Technology Co., Ltd., Shanghai, China). In addition to pharmacokinetic parameters such as C_{\max} , t_{\max} and AUC, F_a was calculated by deconvolution using the Wagner–Nelson method for a one-compartmental model in Eq. (3):

$$F_a = \frac{(C_t + k\text{AUC}_{0 \rightarrow t})}{k\text{AUC}_{0 \rightarrow \infty}} \times 100\% \quad (3)$$

where C_t is the drug plasma concentration at time t , AUC is the area under the curve, and k is the elimination rate constant.

A point-to-point correlation between F_a and *in vivo* dissolution or *in vitro* dissolution, as obtained in Sections 2.6 and 2.7, was investigated. For ease of comparison, all data were presented as percent of residual FNB-HCs.

3. Results and discussion

3.1. Characterization of FNB-HCs

The physicochemical properties of FNB-HCs are summarized in Table 1. The D_{90} of FNB-HCs is $7.33 \pm 0.64 \mu\text{m}$, which is similar to the commercial FNB preparation Lipanthyl® ($<10 \mu\text{m}$)⁶⁴. The EE (%) and DL (%) of P2 in FNB-HCs is $25.98 \pm 0.32\%$ and $0.02 \pm 0.01\%$, respectively. The fluorescence intensity of FNB-HCs is strong enough for *in vivo* imaging owing to the high quantum yield of P2^{57,58}. Owing to the extremely low loading of the dye, the morphology and crystallographic properties of FNB do not change significantly (Fig. 2). FNB-HCs present as bulk crystals with a size much smaller than that of FNB raw crystals (Fig. 2A and B). DSC thermograms show an endothermic peak at 84°C for both FNB and FNB-HCs (Fig. 2D), representing the melting point of FNB^{65,66}. The PXRD diffractograms show characteristic diffraction peaks at 2° , 11° , 20° , 21° , 25° , 30° and 34° for FNB-HCs, which is consistent with FNB raw crystals (Fig. 2E). It is concluded that FNB-HCs retain physical properties similar to FNB raw crystals except particle size.

3.2. Fluorescence stability and sensitivity to water

To precisely and sensitively monitor the dissolution of FNB-HCs, the dyes should be securely embedded inside the crystal lattices, while the fluorescence should quench instantly and completely upon dissolution of the crystals. The fluorescence stability of FNB-HCs and the sensitivity to water were thus validated.

The very good fluorescence stability of FNB-HCs in pure water and all buffers of different pHs (Fig. 3A) indicates a lack of dye leakage or water infiltration into the crystal lattices, both of which could lead to false signals owing to premature quenching^{41,67}. With regard to fasted-state simulated small intestine fluid (FaSSIF) and fed-state simulated small intestine fluid (FeSSIF), the fluorescence decreases to 90% and 75% of the original after 12 h (Fig. 3B), respectively. Nevertheless, it does not mean dye leakage or water infiltration. It is mainly due to the presence of surfactants—generally phospholipids and bile salts—in both FaSSIF and FeSSIF that solubilize FNB-HCs and thereby lead to gradual decrease of fluorescence. As FeSSIF is fortified with more surfactants than FaSSIF, more FNB-HCs dissolve in FeSSIF than in FaSSIF, resulting in lower levels of residual fluorescence in FeSSIF (Fig. 3B). The fact of much stable fluorescence in simulated gastric fluid (SGF) serves as a counter-evidence to support the observations in FeSSIF because SGF does not contain any surfactants. Simultaneous monitoring of FNB gives synchronous dissolution behaviors (Fig. 3C and D). The fluorescent quenching should be ascribed to the dissolution of FNB-HCs, rather than dye leakage or water infiltration. Therefore, fluorescence quenching is justified as a measure to determine dissolution of FNB-HCs.

Table 1 Physicochemical properties of FNB-HCs and FNB raw crystals (mean \pm SD, $n = 3$).

	Size (μm)			Span	EE (%)	DL (%)	TRE [(p/s)/($\mu\text{W}/\text{cm}^2$) $\times 10^{-9}$]
	D_{10}	D_{50}	D_{90}				
FNB-HC	3.2 ± 0.2	4.8 ± 0.4	7.3 ± 0.6	0.8 ± 0.03	26.98 ± 0.32	0.02 ± 0.01	4.58 ± 0.17
FNB	80.3 ± 33.5	131.5 ± 28.5	215.3 ± 30.6	1.1 ± 0.3			

D_{10} , D_{50} and D_{90} refer to the diameter below which there are 10%, 50% and 90% of particles.

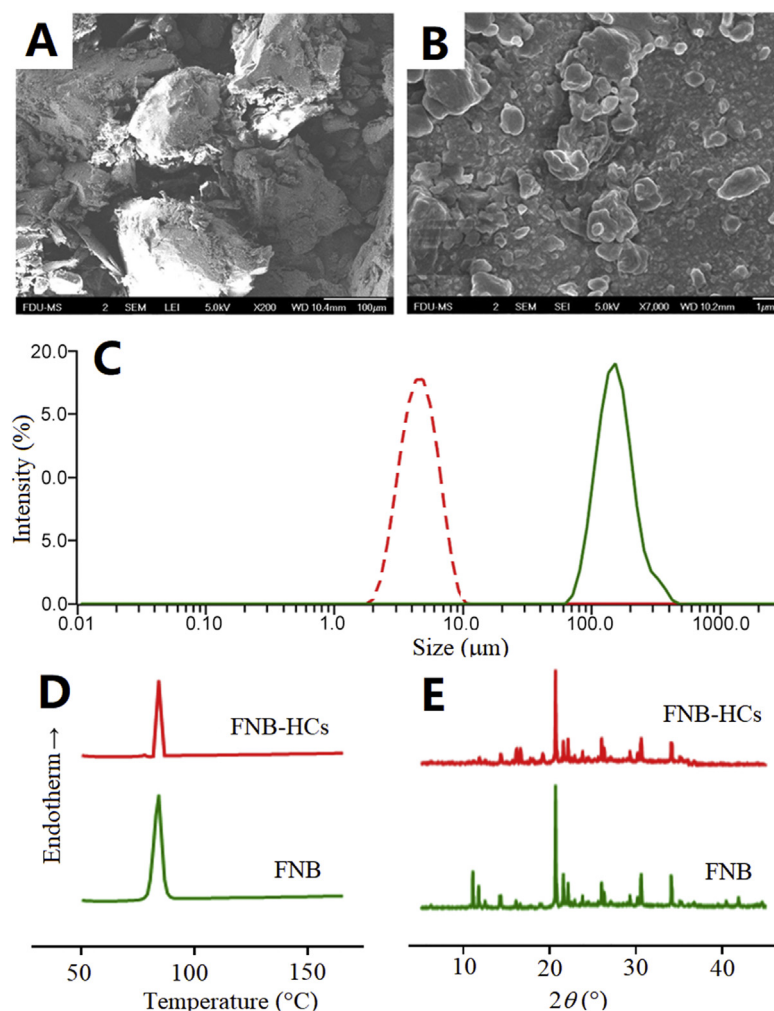


Figure 2 SEM photographs of FNB raw material (A) and FNB-HCs (B); size distribution of FNB raw crystals and FNB-HCs (C); DSC thermograms (D); powder X-ray diffractograms (E).

The fluorescence spectra of FNB-HCs dissolved in aqueous ethanol is shown in Fig. 3E. The fluorescence decreases as a function of water content and quenches completely at a turning point of 70% (Fig. 3F). It stands to reason that the fluorescence of FNB-HCs is able to quench absolutely upon dissolution in the aqueous biological environment.

3.3. *In vitro* dissolution

In vitro dissolution was first determined by measuring FNB in the dissolution medium following conventional monograph protocol. To facilitate comparison with fluorescence quenching, the dissolution profile is expressed as undissolved residual drug *vs.* time by deducting the percentages of dissolved FNB from 100% (Fig. 4A, red line), rather than a routine display of accumulative dissolved percentages. The residual amount of FNB-HCs was quantified based on residual fluorescence according to a calibration curve (Supporting Information Fig. S2). Linearity was observed between fluorescence intensity and undissolved FNB-HCs within the concentration range of 2.10–135 μg/mL ($r = 0.9994$). The accuracy was between 95% and 105% for samples of low, medium and high concentrations, and the precision was less than 6% for both within-day and between-day assays (Supporting Information Tables S1 and S2). The

fluorescence-based dissolution profile is shown in Fig. 4A (blue line). Good correlation ($r = 0.9824$) is observed between the two *in vitro* dissolution profiles measured by monitoring either dissolved FNB or fluorescence (Fig. 4B).

The quantitative correlation is based on stable embedment of ACQ dyes in the FNB crystalline lattices and sensitive water-quenching capability. Along with dissolution of FNB-HCs, the ACQ dyes are released into an aqueous environment and quench absolutely due to self-aggregation, while the embedded ACQ dyes in residual FNB-HCs still remain emissive. As revealed in the stability study, no dye leakage and water infiltration that could result in false signals are recorded. The fluorescence signals can be used to identify and measure FNB-HCs.

The finding here, together with that observed in the stability study, proves the synchronicity between FNB dissolution and fluorescence quenching, which establishes the basis for further investigation of dissolution by real-time monitoring of residual particle-associated fluorescence.

3.4. *In vivo* dissolution

Fig. 5A shows the live images of SD rats after oral administration of FNB-HCs by gavage. Almost no fluorescence signals discriminable from the background were found in rats treated with

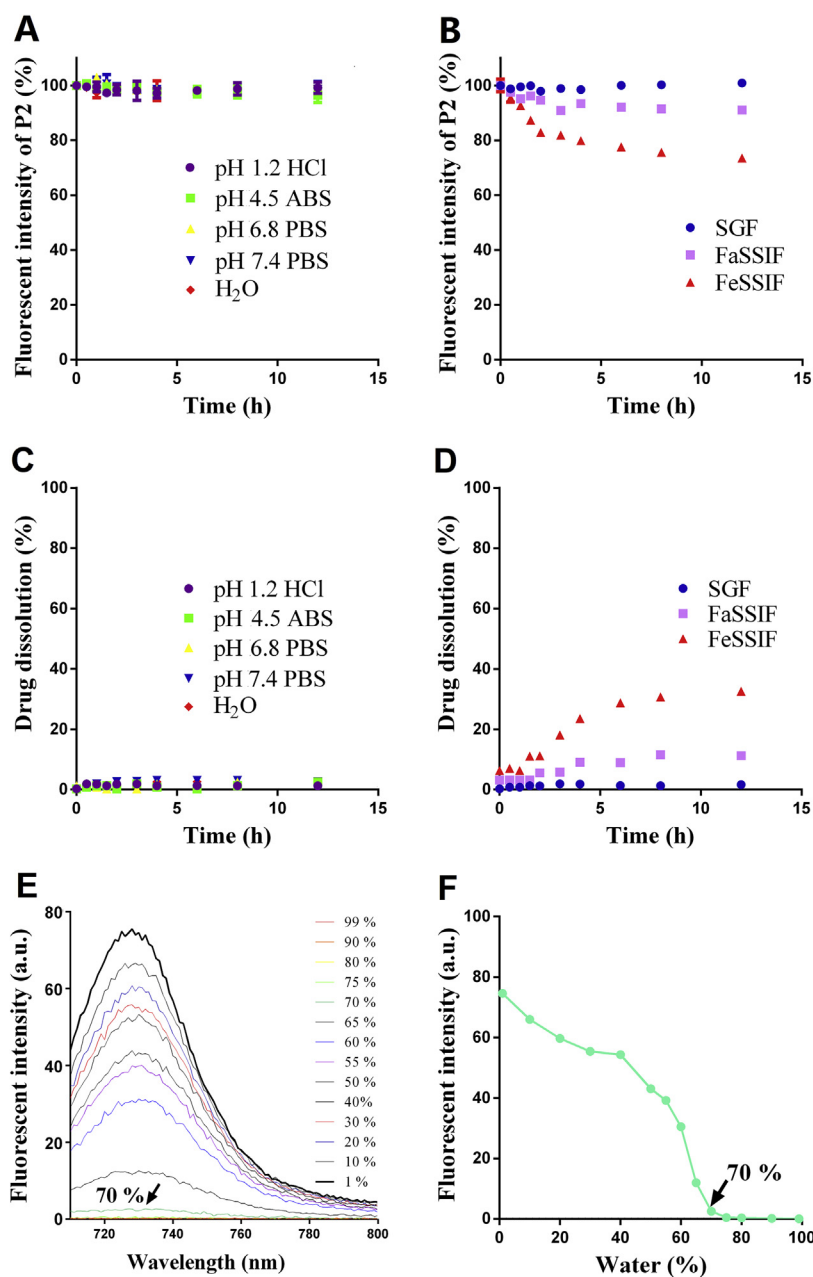


Figure 3 *In vitro* fluorescent stability of FNB-HCs in buffers of different pHs (ABS; acetate buffered saline; PBS: phosphate buffered saline) and pure water (A) and in different bio-relevant fluids (B). SGF, simulated gastric fluid; FeSSIF, fed-state simulated small intestinal fluid; FaSSIF, fasted-state simulated small intestinal fluids. Validation of dissolution by measuring the drug: in buffers and water (C); in different bio-relevant fluids (D). Data are expressed as mean \pm SD ($n = 3$). Fluorescent spectra of FNB-HCs in aqueous ethanol (E) and the plot of fluorescent intensity vs. water content (F).

pre-quenched P2 dispersion, indicating little fluorescence reillumination (Supporting Information Fig. S3). For the rats treated with FNB-HCs, the signals mainly locate to the abdominal region. The fluorescence shows a declining trend and disappears at 60 min post administration, indicating gradual dissolving of FNB-HCs. In view that the fluorescence represents residual FNB-HCs, the *in vivo* dissolution profile is thus delineated from the residual percentage of fluorescence with the initial value set to 100% (Fig. 5B, blue line) and compared with the *in vitro* dissolution

profile (Fig. 5B, red line). A not-too-bad correlation is established with a correlation coefficient of 0.90 (Fig. 5C).

Considering the limited tissue penetration of fluorescence, the whole GIT were dissected for IVIS imaging after sacrificing the animals at each time point (Fig. 6A). The pre-quenched P2 control exhibits little fluorescence as well, confirming negligible interference due to reillumination (Supporting Information Fig. S4). The fluorescence of residual FNB-HCs resides mainly in the stomach during the period of observation and attenuates with time.

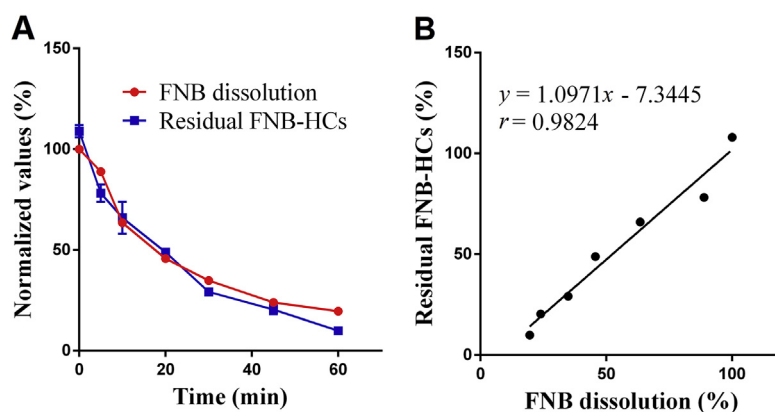


Figure 4 *In vitro* dissolution of FNB-HCs determined by monitoring either FNB (red line) or fluorescence (A, blue line) and correlation (B) that highlight synchronicity between drug dissolution and fluorescence quenching. Data are expressed as mean \pm SD ($n = 3$).

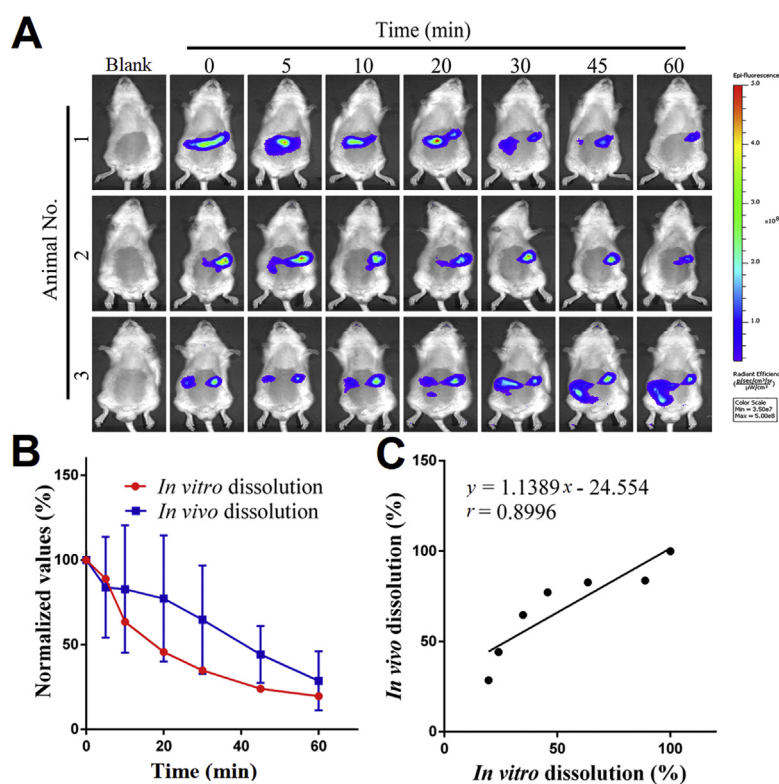


Figure 5 *In vivo* dissolution based on live imaging of residual FNB-HCs. Live images of SD rats after oral administration of FNB-HCs gavage (A). Comparison of *in vivo* dissolution profile obtained from residual percentage of fluorescent intensity (blue line) with the *in vitro* dissolution profile (B, red line) and IVIVC established between them (C). Data are expressed as mean \pm SD ($n = 3$).

At 60 min, the fluorescence almost disappears due to fast dissolution of micronized FNB crystals⁶⁸. The *ex vivo* results comply with that obtained by live imaging (Fig. 5A). Similarly, the residual percentage of fluorescence intensity in the stomach vs. time is employed to plot the *in vivo* dissolution profiles (Fig. 6B, blue line). Very good correlation is observed between *in vivo* and *in vitro* dissolution profile (Fig. 6B, red line) with a correlation coefficient of 0.95 (Fig. 6C). Although *ex vivo* imaging confirms the results of live imaging, the latter is however preferred for ease of handling, monitoring in real time and not needing to sacrifice a large number of animals.

3.5. Validation by IVIVC with F_a

Since FNB is rapidly metabolized into fenofibric acid and unmeasurable in plasma, pharmacokinetics of FNB were evaluated based on plasma concentration of fenofibric acid⁶². The plasma fenofibric acid concentration vs. time profile after oral administration of FNB-HCs is shown in Fig. 7A. The plasma fenofibric acid concentration increases rapidly and reaches a maximum at around 1 h post administration due to the quick dissolution of FNB in the stomach (Figs. 5 and 6). The main pharmacokinetic parameters of oral FNB-HCs are shown in Table 2. Results indicate

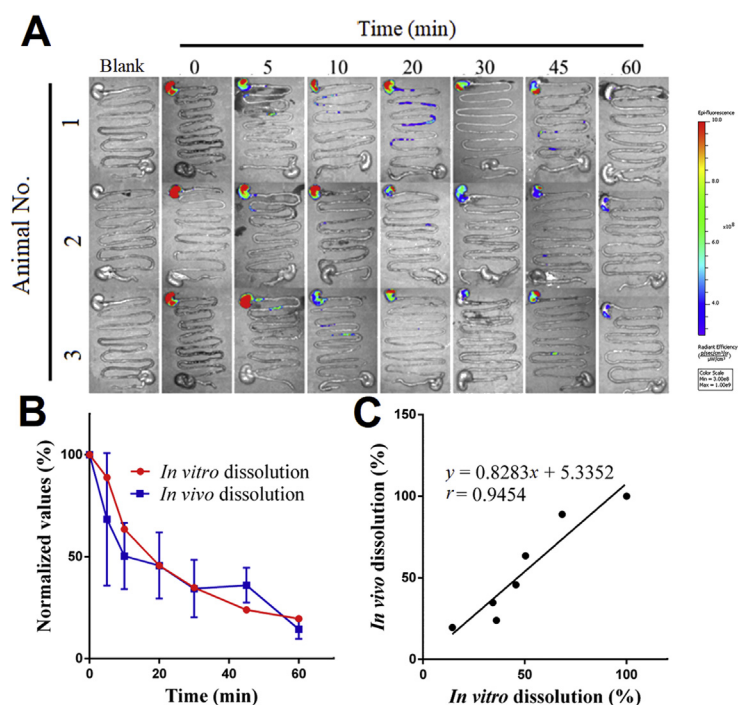


Figure 6 *In vivo* dissolution based on *ex vivo* imaging of residual FNB-HCs. *Ex vivo* images of the whole isolated GI segments after oral administration of FNB-HCs by gavage (A). Comparison of the *in vivo* dissolution profile obtained from residual percentage of fluorescent intensity in the stomach (blue line) and the *in vitro* dissolution (B, red line) and IVIVC established between them (C). Data are expressed as mean \pm SD ($n = 3$).

that the plasma levels of fenofibric acid increase quickly after administration by gavage, with a C_{max} of 13.22 $\mu\text{g/mL}$ at 1.17 h. The value of T_{max} is comparable to that of the commercial product Lipanthyl®^{69,70}.

The *in vivo* F_a of FNB-HCs was calculated *via* Eq. (3) and plotted *vs.* time (Fig. 7B). One compartmental model was determined based on the criterion of minimum AIC given by the pharmacokinetic software (DAS 2.0, Shanghai, China). Therefore, deconvolution by the Wagner–Nelson method for one-compartment model is applicable for the calculation of F_a . Under fed state, F_a of FNB-HCs reaches a maximum of 114% in approximately 60 min, and the F_a profile correlates very well with the *in vitro* dissolution profile with a correlation coefficient of 0.94 (Fig. 7C), confirming a level-A IVIVC according to FDA guidelines^{71,72}. Being a BCS Class II drug with good permeability, F_a reflects the *in vivo* dissolution of FNB. Therefore, the *in vivo* dissolution profile also correlates very well with the F_a profile with a correlation coefficient of 0.97 (Fig. 7D). The good correlation among *in vitro* dissolution, *in vivo* dissolution and *in vivo* F_a strengthens the applicability of *in vivo* dissolution for establishment of IVIVC.

4. General discussion

In vivo dissolution is not a new concept. Both administrative agencies and academics have called on investigations into it, aiming to realize authentic IVIVC^{18–20}. However, previous endeavors failed due to a lack of workable tools to monitor either dissolved drugs or residual drug particles as a whole in real time, based on which the *in vivo* dissolution percentages could be calculated. This article is probably the first report on *in vivo*

dissolution profiles based on measurement of residual drug particles, as well as the realization of IVIVC between *in vitro* and *in vivo* dissolution. The high correlation coefficient ($r = 0.8996$) observed in this study between *in vitro* and *in vivo* dissolution stands for a Level A point-to-point IVIVC according to FDA guidelines^{18,19}. The newly established IVIVC is further validated by the conventional IVIVC protocol—correlation with F_a —calculated from the pharmacokinetic profiles. Level A IVIVC has been established for FNB formulations between *in vitro* dissolution and F_a by previous studies^{22,54–56} and the current study confirms previous findings. The fact that good IVIVC exists between *in vivo* dissolution and F_a strengthens the newly established IVIVC between *in vitro* and *in vivo* dissolution.

It is not hard to understand that ready absorption of the APIs in the GIT is a prerequisite for a conventional F_a -based IVIVC study. Apparently, it is impractical to expect high-level IVIVC from Class III and IV compounds because of limited and irregular absorption owing to poor permeability. Although F_a of poorly permeable drugs can be measured as well, the value is too limited to be utilized to establish IVIVC. Therefore, the overall success rate for Class III and IV drugs is very low. The conclusions of this study suggest that future IVIVC may be established between *in vitro* and *in vivo* dissolution profiles instead of *in vitro* dissolution and F_a . The newly proposed protocol may help evade the absorption uncertainties associated with poorly permeable drugs. IVIVC should reflect both pharmaceutical and biopharmaceutical behaviors of drugs in the GIT, but not only its absorption. It is envisioned that the acceptance rate of IVIVC for Class III and IV drugs would be highly increased if *in vivo* dissolution is employed to investigate IVIVC by administrative agencies.

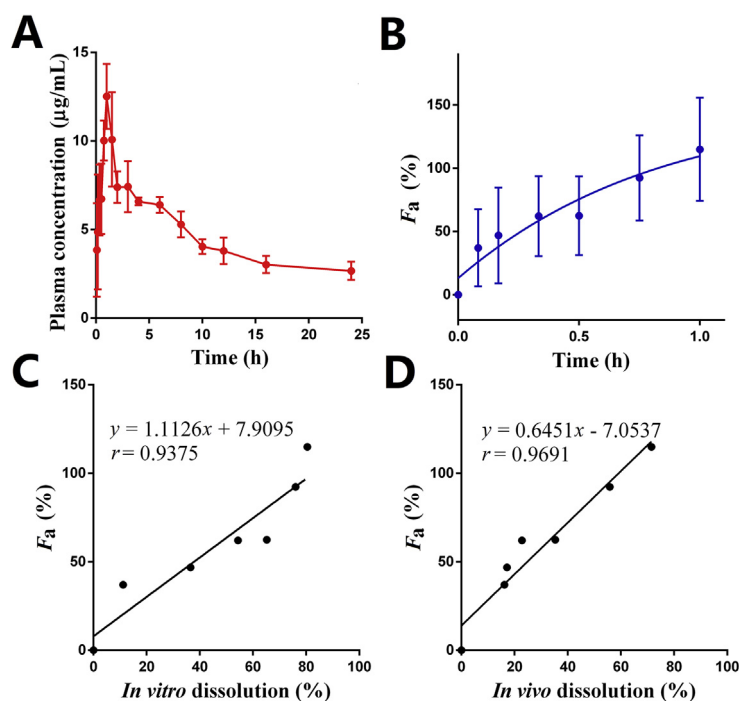


Figure 7 Mean plasma concentration of fenofibric acid vs. time plot in rats post administration of FNB-HCs by gavage (A); normalized values of F_a vs. time (B); correlation between F_a and *in vitro* dissolution (C); correlation between F_a and *in vivo* dissolution (D). Data are expressed as mean \pm SD ($n = 5$).

Table 2 Main pharmacokinetic parameters of fenofibric acid post oral administration of FNB-HCs by gavage.

PK parameter	Value ^a
C_{max} ($\mu\text{g/mL}$)	13.22 ± 1.30
T_{max} (h)	1.17 ± 0.29
$AUC_{0-\infty}$ ($\mu\text{g}\cdot\text{h/mL}$)	184.72 ± 54.11
K (1/h)	0.07 ± 0.01

^aData are mean \pm SD, $n = 5$.

FNB is chosen as the model drug because it is a highly permeable drug (Class II) with well-established IVIVC^{22,54–56}, a feather that can be utilized to validate the *in vitro/in vivo* dissolution correlation hypothesis. On the other hand, the poor water-solubility of FNB grants temporal flexibility for the measurement of *in vivo* dissolution based on fluorescence. We also tested propranolol, a Class I drug, that is highly water-soluble and permeable with well-established IVIVC (see [Supporting Information](#)). Unfortunately, the drug dissolves so quickly in the GIT that we failed to capture sufficient data because data collection demands more time than actually allowed. In this study, we just showcase the proof of concept of *in vivo* dissolution by using FNB. It is highly expectable to expand the concept to more model drugs ranging from Class I to Class IV.

In this study, the proof of concept of *in vivo* dissolution as well as the IVIVC based on it has been validated, but there is still a long way ahead to put the concepts into practical use. There are a few obstacles yet to be overcome. It should be noted that all experiments have been carried out in rats. There are so far no similar or alternative methods available for human studies. On the other hand, in live imaging, the light must penetrate the body tissues

first, which may absorb a majority of the energy and possess auto-fluorescence that interferes with live imaging. To reduce such interference, NIR region II dyes (1000–1700 nm) with higher penetration and less tissue auto-fluorescence might be a better choice to replace NIR region I dyes in future studies^{73,74}.

The investigation of *in vivo* dissolution is meant to provide guidance for the screening of *in vitro* dissolution protocols based on establishment of IVIVC. In this study, we did not perform screening of *in vitro* dissolution conditions but employed pharmacopeia method with well-established and documented IVIVC. On the contrary, the current IVIVC is used to test *in vivo* dissolution as a measure to establish authentic IVIVC. Although the pharmacopeia method has been developed according to human data, it is well replicated in the current rat model. It is expected that in the future *in vivo* dissolution profiles can be used as a standard to screen *in vitro* dissolution conditions. It is also very interesting to notice that the efficient of *in vivo* dissolution vs. F_a ($r = 0.9691$) correlation is higher than that of *in vitro* dissolution vs. F_a ($r = 0.9375$), which implies that the current *in vitro* dissolution protocols for FNB might not be an ideal one and there are still margins for improvement.

The currently running IVIVC protocols acceptable in regulatory agencies is solely based on a makeshift correlation between *in vitro* dissolution and F_a . As F_a is subject to various factors that influence the absorption and systemic exposure of APIs, IVIVC of conventional practice can be established only when proportional correlation exists between virtual *in vivo* dissolution and F_a . Nevertheless, irregular or erroneous absorption, which is common for BCS III and IV drugs, hinders the successful establishment of IVIVC. The current low acceptance rate bespeaks the bottleneck of current IVIVC practices. If *in vivo* dissolution is able to be measured with accuracy, regulatory agencies would like to accept the new *in vitro–in vivo* dissolution IVIVC protocol because it is

direct and authentic correlation between dissolution profiles. Owing to limitations with the bioimaging strategy used in this study, we only provide the proof of concept of *in vivo* dissolution-based IVIVC. The procedures employed in this study are not meant to be used universally for other models but calls for more investigation on the concepts and protocols involved. The application of *in vivo* dissolution concept in IVIVC is expectable if accurate measurement of *in vivo* dissolution in humans comes into truth in the future.

5. Conclusions

The concept of *in vivo* dissolution is proved with FNB as a model for poorly water-soluble drug based on real-time monitoring of residual or undissolved drug crystals in GIT. In order to identify and measure FNB crystals, an NIR fluorophore, P2, suitable for non-invasive live imaging is utilized to label FNB crystals through recrystallization. The complete and instant quenching of fluorescence upon dissolving and release into aqueous media justifies the accurate identification of FNB-HCs both *in vitro* and *in vivo*. The fluorescence stability of FNB-HCs in buffers and bio-relevant media indicates no dye leakage and water infiltration, which may compromise the accuracy of bioimaging. Linearity between crystal-borne fluorescence and residual crystal amount is established ($r = 0.9824$) for the quantification of FNB-HCs. *In vitro* dissolution is studied under pharmacopeia conditions by monitoring either FNB or fluorescence, and very good correlation exist between dissolution profiles acquired by the two approaches, confirming the reliability of using fluorescence to monitor crystal dissolution. *In vivo* dissolution is first investigated by live imaging and results indicate fast and complete dissolution in the stomach within 60 min. Correlation of *in vivo* with *in vitro* dissolution profile gives a coefficient of 0.8996, implying a level A point-to-point correlation according to FDA guidelines. Elevated correlation levels with a coefficient of 0.9454 are observed between *in vivo* dissolution acquired in *ex vivo* GIT and *in vitro* dissolution. Both live and *ex vivo* imaging results of *in vivo* dissolution validate the correctness of the current pharmacopeia *in vitro* dissolution protocols. The correlation between F_a and *in vitro* dissolution ($r = 0.9375$) confirms the well established Level A IVIVC, whereas the higher correlation coefficient of 0.9691 between F_a and *in vivo* dissolution validates the potential application of *in vivo* dissolution for the establishment of authentic IVIVC.

Acknowledgments

This work was supported by the National Natural Science Foundation of China (Nos. 81973247, 81872815, 81872826 and 81690263) and Science and Technology Commission of Shanghai Municipality (19XD1400300, China). We are grateful for Prof. Dr. Yu-Kyoung Oh of Seoul National University Nano Biodrug Delivery Lab for the illuminating comments she provided.

Author contributions

Wei Wu and Yi Lu designed the research. Yinqian Yang carried out the experiments and performed data analysis. Yongjiu Lv, Chengying Shen, Tingting Shi and Haisheng He participated in part of the experiments. Weili Zhao and Xiaochun Dong provided experimental drugs and quality control. Yinqian Yang wrote the manuscript. Wei Wu, Yi Lu and Jianping Qi revised the

manuscript. All of the authors have read and approved the final manuscript.

Conflicts of interest

The authors have no conflicts of interest to declare.

Appendix A. Supporting information

Supporting data to this article can be found online at <https://doi.org/10.1016/j.apsb.2020.08.002>.

References

- Allen Jr LV, Popovich NG, Aansel HC. *Ansel's pharmaceutical dosage forms and drug delivery systems*. 8th ed. Baltimore: Lippincott Williams & Wilkins; 2013.
- Shargel L, Yu ABC. *Applied biopharmaceutics & pharmacokinetics*. 7th ed. New York: McGraw-Hill Education; 2016.
- Guo M, Wei M, Li W, Guo M, Guo C, Ma M, et al. Impacts of particle shapes on the oral delivery of drug nanocrystals: mucus permeation, transepithelial transport and bioavailability. *J Control Release* 2019; **307**:64–75.
- Fu Q, Sun J, Ai X, Zhang P, Li M, Wang Y, et al. Nimodipine nanocrystals for oral bioavailability improvement: role of mesenteric lymph transport in the oral absorption. *Int J Pharm* 2013; **448**:290–7.
- Xie Y, Shi B, Xia F, Qi J, Dong X, Zhao W, et al. Epithelia transmembrane transport of orally administered ultrafine drug particles evidenced by environment sensitive fluorophores in cellular and animal studies. *J Control Release* 2018; **270**:65–75.
- Shen C, Yang Y, Shen B, Xie Y, Qi J, Dong X, et al. Self-discriminating fluorescent hybrid nanocrystals: efficient and accurate tracking of translocation via oral delivery. *Nanoscale* 2017; **10**:436–50.
- Sugano K, Terada K. Rate- and extent-limiting factors of oral drug absorption: theory and applications. *J Pharm Sci* 2015; **104**:2777–88.
- Shi Q, Moinuddin SM, Cai T. Advances in coamorphous drug delivery systems. *Acta Pharm Sin B* 2019; **9**:19–35.
- Cook JA. A technique to estimate *in vivo* dissolution profiles without data from a solution. *AAPS J* 2012; **14**:433–6.
- Kostewicz ES, Abrahamsson B, Brewster M, Brouwers J, Butler J, Carlet S, et al. *In vitro* models for the prediction of *in vivo* performance of oral dosage forms. *Eur J Pharmaceut Sci* 2014; **57**:342–66.
- Bou-Chacra N, Melo KJC, Morales IAC, Stippler ES, Kesisoglou F, Yazdani M, et al. Evolution of choice of solubility and dissolution media after two decades of Biopharmaceutical Classification System. *AAPS J* 2017; **19**:989–1001.
- Charalabidis A, Sfouni M, Bergstrom C, Macheras P. The biopharmaceutics classification system (BCS) and the biopharmaceutics drug disposition classification system (BDDCS): beyond guidelines. *Int J Pharm* 2019; **566**:264–81.
- Hens B, Sinko PD, Job N, Dean M, Al-Gousous J, Salehi N, et al. Formulation predictive dissolution (fPD) testing to advance oral drug product development: an introduction to the US FDA funded '21st Century BA/BE' project. *Int J Pharm* 2018; **548**:120–7.
- Kaur N, Narang A, Bansal AK. Use of biorelevant dissolution and PBPK modeling to predict oral drug absorption. *Eur J Pharm Biopharm* 2018; **129**:222–46.
- Emami J. *In vitro*–*in vivo* correlation: from theory to applications. *J Pharm Pharmaceut Sci* 2006; **9**:169–89.
- Ruiz Picazo A, Martinez-Martinez MT, Colon-Useche S, Iriarte R, Sanchez-Dengra B, Gonzalez-Alvarez M, et al. *In vitro* dissolution as a tool for formulation selection: telmisartan two-step IVIVC. *Mol Pharm* 2018; **15**:2307–15.
- Suarez-Sharp S, Li M, Duan J, Shah H, Seo P. Regulatory experience with *in vivo* *in vitro* correlations (IVIVC) in new drug applications. *AAPS J* 2016; **18**:1379–90.

18. U.S. Food and Drug Administration. Guidance for industry-extended release oral dosage forms-development, evaluation and application of *in vitro*-*in vivo* correlations. Available from: <https://www.fda.gov/regulatory-information/search-fda-guidance-documents/extended-release-oral-dosage-forms-development-evaluation-and-application-vitro-in-vivo-correlations>. [Accessed 16 April 2020].
19. U.S. Food and Drug Administration. Waiver on *in vivo* bioavailability and bioequivalence studies for immediate-release solid oral dosage forms based on a Biopharmaceutics classification systems. Available from: <https://www.fda.gov/regulatory-information/search-fda-guidance-documents/waiver-vivo-bioavailability-and-bioequivalence-studies-immediate-release-solid-oral-dosage-forms>. [Accessed 16 April 2020].
20. Lu Y, Kim S, Park K. *In vitro*-*in vivo* correlation: perspectives on model development. *Int J Pharm* 2011;**418**:142–8.
21. Kytariolos J, Dokoumetzidis A, Macheras P. Power law IVIVC: an application of fractional kinetics for drug release and absorption. *Eur J Pharmaceut Sci* 2010;**41**:299–304.
22. Xu H, Shi Y, Vela S, Marroum P, Gao P. Developing quantitative *in vitro*-*in vivo* correlation for fenofibrate immediate-release formulations with the biphasic dissolution-partition test method. *J Pharm Sci* 2018;**107**:476–87.
23. Wagner JG. Estimation of theophylline absorption rate by means of the Wagner–Nelson equation. *J Allergy Clin Immunol* 1986;**78**:681–8.
24. Wagner JG. Effect of using an incorrect elimination rate constant in application of the Wagner–Nelson method to theophylline data in cases of zero order absorption. *Biopharm Drug Dispos* 1984;**5**:75–83.
25. Ostrowski M, Wilkowska E, Baczek T. The influence of averaging procedure on the accuracy of IVIVC predictions: immediate release dosage form case study. *J Pharm Sci* 2010;**99**:5040–5.
26. Wang Y, Nedelman J. Bias in the Wagner-Nelson estimate of the fraction of drug absorbed. *Pharm Res (N Y)* 2002;**19**:470–6.
27. Cardot JM, Davit BM. *In vitro*-*in vivo* correlations: tricks and traps. *AAPS J* 2012;**14**:491–9.
28. Kaur P, Jiang X, Duan J, Stier E. Applications of *in vitro*-*in vivo* correlations in generic drug development: case studies. *AAPS J* 2015;**17**:1035–9.
29. Nguyen MA, Flanagan T, Brewster M, Kesiosoglou F, Beato S, Biewenga J, et al. A survey on IVIVC/IVIVR development in the pharmaceutical industry—past experience and current perspectives. *Eur J Pharmaceut Sci* 2017;**102**:1–13.
30. Lennernas H, Lindahl A, Van Peer A, Ollier C, Flanagan T, Lionberger R, et al. *In vivo* predictive dissolution (IPD) and biopharmaceutical modeling and simulation: future use of modern approaches and methodologies in a regulatory context. *Mol Pharm* 2017;**14**:1307–14.
31. Roudier B, Davit B, Schutz H, Cardot JM. Impact of data base structure in a successful *in vitro*-*in vivo* correlation for pharmaceutical products. *AAPS J* 2015;**17**:24–34.
32. Brouwers J, Augustijns P. Resolving intraluminal drug and formulation behavior: gastrointestinal concentration profiling in humans. *Eur J Pharmaceut Sci* 2014;**61**:2–10.
33. Hens B, Corsetti M, Spiller R, Marciani L, Vanuytsel T, Tack J, et al. Exploring gastrointestinal variables affecting drug and formulation behavior: methodologies, challenges and opportunities. *Int J Pharm* 2017;**519**:79–97.
34. Butler J, Hens B, Vertzoni M, Brouwers J, Berben P, Dressman J, et al. *In vitro* models for the prediction of *in vivo* performance of oral dosage forms: recent progress from partnership through the IMI OrBiTo collaboration. *Eur J Pharm Biopharm* 2019;**136**:70–83.
35. Knutson PFT, Ahlström H, Magnusson A, Tannergren C, Lennerna H. Increased understanding of intestinal drug permeability determined by the LOC-I-GUT approach using multislice computed tomography. *Mol Pharm* 2008;**6**:2–10.
36. Petri N, Tannergren C, Holst B, Mellon FA, Bao Y, Plumb GW, et al. Absorption/metabolism of sulforaphane and quercetin, and regulation of phase II enzymes, in human jejunum *in vivo*. *Drug Metab Dispos* 2003;**31**:805–13.
37. Brouwers J, Ingels F, Tack J, Augustijns P. Determination of intraluminal theophylline concentrations after oral intake of an immediate- and a slow-release dosage form. *J Pharm Pharmacol* 2005;**57**:987–96.
38. Koenigsnecht MJ, Baker JR, Wen B, Frances A, Zhang H, Yu A, et al. *In vivo* dissolution and systemic absorption of immediate release ibuprofen in human gastrointestinal tract under fed and fasted conditions. *Mol Pharm* 2017;**14**:4295–304.
39. Bergstrom CA, Holm R, Jorgensen SA, Andersson SB, Artursson P, Beato S, et al. Early pharmaceutical profiling to predict oral drug absorption: current status and unmet needs. *Eur J Pharmaceut Sci* 2014;**57**:173–99.
40. Bermejo M, Paixão P, Hens B, Tsume Y, Koenigsnecht MJ, Baker JR, et al. Linking the gastrointestinal behavior of ibuprofen with the systemic exposure between and within humans—part I: fasted state conditions. *Mol Pharm* 2018;**15**:5454–67.
41. Lu Y, Lv Y, Li T. Hybrid drug nanocrystals. *Adv Drug Deliv Rev* 2019;**143**:115–33.
42. Qi J, Hu X, Dong X, Lu Y, Lu H, Zhao W, et al. Towards more accurate bioimaging of drug nanocarriers: turning aggregation-caused quenching into a useful tool. *Adv Drug Deliv Rev* 2019;**143**:206–25.
43. Wang L, Liu M, Chen Y. Carbon dots and terbium co-enhanced fluorescence of europium nanoparticles for cell Imaging. *J Biomed Nanotechnol* 2018;**14**:1898–905.
44. Wang B, Lv P, Cai H, Li Y, Zhu H, Lui S, et al. Enzyme-responsive copolymer as a theranostic prodrug for tumor *in vivo* imaging and efficient chemotherapy. *J Biomed Nanotechnol* 2019;**15**:1897–908.
45. Hu D, Chen L, Qu Y, Peng J, Chu B, Hao Y, et al. Oxygen-generating hybrid polymeric nanoparticles with encapsulated doxorubicin and chlorin e6 for trimodal imaging-guided combined chemophotodynamic therapy. *Theranostics* 2018;**8**:1558–74.
46. Wang Y, Zhang Y, Wang J, Liang XJ. Aggregation-induced emission (AIE) fluorophores as imaging tools to trace the biological fate of nano-based drug delivery systems. *Adv Drug Deliv Rev* 2019;**143**:161–76.
47. Chen T, He B, Tao J, He Y, Deng H, Wang X, et al. Application of Förster resonance energy transfer (FRET) technique to elucidate intracellular and *in vivo* biofate of nanomedicines. *Adv Drug Deliv Rev* 2019;**143**:177–205.
48. Hu X, Zhang J, Yu Z, Xie Y, He H, Qi J, et al. Environment-responsive aza-BODIPY dyes quenching in water as potential probes to visualize the *in vivo* fate of lipid-based nanocarriers. *Nanomedicine* 2015;**11**:1939–48.
49. Hu X, Fan W, Yu Z, Lu Y, Qi J, Zhang J, et al. Evidence does not support absorption of intact solid lipid nanoparticles *via* oral delivery. *Nanoscale* 2016;**8**:7024–35.
50. Hu X, Dong X, Lu Y, Qi J, Zhao W, Wu W. Bioimaging of nanoparticles: the crucial role of discriminating nanoparticles from free probes. *Drug Discov Today* 2017;**22**:382–7.
51. Ahmad E, Feng Y, Qi J, Fan W, Ma Y, He H, et al. Evidence of nose-to-brain delivery of nanoemulsions: cargoes but not vehicles. *Nanoscale* 2017;**9**:1174–83.
52. Xia F, Fan W, Jiang S, Ma Y, Lu Y, Qi J, et al. Size-dependent translocation of nanoemulsions *via* oral delivery. *ACS Appl Mater Interfaces* 2017;**9**:21660–72.
53. He H, Zhang J, Xie Y, Lu Y, Qi J, Ahmad E, et al. Bioimaging of intravenous polymeric micelles based on discrimination of integral particles using an environment-responsive probe. *Mol Pharm* 2016;**13**:4013–9.
54. Pestieau A, Lebrun S, Cahay B, Brouwers A, Streel B, Cardot JM, et al. Evaluation of different *in vitro* dissolution tests based on level A *in vitro*-*in vivo* correlations for fenofibrate self-emulsifying lipid-based formulations. *Eur J Pharm Biopharm* 2017;**112**:18–29.
55. Zuo B, Sun Y, Li H, Liu X, Zhai Y, Sun J, et al. Preparation and *in vitro/in vivo* evaluation of fenofibrate nanocrystals. *Int J Pharm* 2013;**455**:267–75.
56. Hens B, Brouwers J, Corsetti M, Augustijns P. Gastrointestinal behavior of nano- and microsized fenofibrate: *in vivo* evaluation in man and *in vitro* simulation by assessment of the permeation potential. *Eur J Pharmaceut Sci* 2015;**77**:40–7.

57. Zhao W, Carreira EM. Conformationally restricted aza-bodipy: a highly fluorescent, stable, near-infrared-absorbing dye. *Angew Chem Int Ed Engl* 2005;**44**:1677–9.
58. Zhao W, Carreira EM. Conformationally restricted aza-BODIPY: highly fluorescent, stable near-infrared absorbing dyes. *Chemistry* 2006;**12**:7254–63.
59. Zhu W, Romanski FS, Meng X, Mitra S, Tomassone MS. Atomistic simulation study of surfactant and polymer interactions on the surface of a fenofibrate crystal. *Eur J Pharmaceut Sci* 2011;**42**:452–61.
60. O'Shea JP, Faisal W, Ruane-O'Hara T, Devine KJ, Kostewicz ES, O'Driscoll CM, et al. Lipidic dispersion to reduce food dependent oral bioavailability of fenofibrate: *in vitro*, *in vivo* and *in silico* assessments. *Eur J Pharm Biopharm* 2015;**96**:207–16.
61. Guichard JP, Blouquin P, Qing Y. A new formulation of fenofibrate: suprabioavailable tablets. *Curr Med Res Opin* 2008;**16**:134–8.
62. Hanafy A, Spahn-Languth H, Vergnault G, Grenier P, Tubic Grozdanis M, Lenhardt T, et al. Pharmacokinetic evaluation of oral fenofibrate nanosuspensions and SLN in comparison to conventional suspensions of micronized drug. *Adv Drug Deliv Rev* 2007;**59**:419–26.
63. Weng T, Qi J, Lu Y, Wang K, Tian Z, Hu K, et al. The role of lipid-based nano delivery systems on oral bioavailability enhancement of fenofibrate, a BCS II drug: comparison with fast-release formulations. *J Nanobiotechnol* 2014;**12**:39.
64. Curtet B, Teillaud E, Reginalt P, inventors. Fournier Innovation et Synergie, assignee. Novel dosage form of fenofibrate. United States patent US No. 4895726. January 23, 1980.
65. Yang L, Shao Y, Han HK. Development of omega-3 phospholipid-based solid dispersion of fenofibrate for the enhancement of oral bioavailability. *Eur J Pharmaceut Sci* 2015;**78**:103–10.
66. Jadhav NV, Vavia PR. Dodecylamine template-based hexagonal mesoporous silica (HMS) as a carrier for improved oral delivery of fenofibrate. *AAPS PharmSciTech* 2017;**18**:2764–73.
67. Yuan H, Zhao W, Wu W. How can aggregation-caused quenching based bioimaging of drug nanocarriers be improved?. *Ther Deliv* 2020;**11**:809–12.
68. Li F, Zheng X, Bao Y, Chen T, Zeng J, Xu X, et al. Fenofibrate modified-release pellets with lag phase and high oral bioavailability. *Drug Des Dev Ther* 2019;**13**:141–51.
69. Bahloul B, Lassoued MA, Seguin J, Lai-Kuen R, Dhotel H, Sfar S, et al. Self-emulsifying drug delivery system developed by the HLB-RSM approach: characterization by transmission electron microscopy and pharmacokinetic study. *Int J Pharm* 2015;**487**:56–63.
70. Juenemann D, Jantratid E, Wagner C, Reppas C, Vertzoni M, Dressman JB. Biorelevant *in vitro* dissolution testing of products containing micronized or nanosized fenofibrate with a view to predicting plasma profiles. *Eur J Pharm Biopharm* 2011;**77**:257–64.
71. González-García I, Mangas-Sanjuán V, Merino-Sanjuán M, Bermejo M. *In vitro in vivo* correlations general concepts methodologies and regulatory applications. *Drug Dev Ind Pharm* 2015;**41**:1935–47.
72. Cardot JM, Beyssac E, Alric M. *In vitro-in vivo* correlation: importance of dissolution in IVIVC. *Dissolution Technol* 2007;**14**:15–9.
73. Antaris AL, Chen H, Cheng K, Sun Y, Hong G, Qu C, et al. A small-molecule dye for NIR-II imaging. *Nat Mater* 2016;**15**:235–42.
74. Cai Y, Wei Z, Song C, Tang C, Han W, Dong X. Optical nano-agents in the second near-infrared window for biomedical applications. *Chem Soc Rev* 2019;**48**:22–37.